Proceedings of IMECE2007
2007 ASME International Mechanical Engineering Congress and Exposition
November 11-15, 2007, Seattle, Washington, USA

IMECE2007-42202

LESSONS LEARNED FROM MATCHING EXPERIMENTAL DATA TO LOW-ORDER MODELS OF VEHICLE YAW, SIDESLIP, AND ROLL BEHAVIOR

Sean N. Brennan
Assistant Professor
Pennsylvania State University
Department of Mechanical Engineering

Bridget C. Hamblin
Research Assistant
Pennsylvania State University
Department of Mechanical Engineering

ABSTRACT

This work presents "lessons learned" from an ongoing experimental and simulation investigation of vehicle chassis motion in yaw, sideslip, and roll. In particular, low-order models and parameter fitting methods are examined to illustrate how different combinations of maneuvers and algorithms can generate inconsistent estimates of key model parameters, particularly cornering stiffness. The key contribution of this study versus that of previous work [5] is the discovery of the source of estimation discrepancies including tire camber effects and terrain influences. Methods to remove both effects are proposed and demonstrated. The resulting roll- and terrain-corrected model fits show a significantly improved fit in the frequency domain and outstanding fit in the time domain.

INTRODUCTION

Accidental death due to motor vehicle accidents claim over 1.2 million life-years of unlived life each year, and is the largest premature death factor for those under the age of 65 [1]. Among the myriad causes of vehicle accidents, rollover stands out as an area deserving of particular focus: while vehicle rollover is involved in only 2.5% of the 11 million accidents a year, it accounts for approximately 20% of all fatalities [2].

Through repeated experimentation, the National Highway Traffic Safety Administration (NHTSA) has developed a number of transient maneuvers that can induce untripped wheel lift or even untripped vehicle rollover in some vehicle models [3, 4]. While this experimental approach is unarguably valid for illustrating shortcomings in vehicle behavior, the method itself has analytical shortcomings. In particular, it is difficult to definitively establish whether roll safety is ensured over all possible transient maneuvers. Additionally, experimental results do not directly translate into a representative vehicle model suitable for rollover mitigation through feedback control. Both factors highly motivate the development of dynamic vehicle models.

In selecting a dynamic model, the complexity should match well with the intended use. This study focuses on suitable models for control synthesis. Hence, the objective is to determine the modifications necessary to improve the accuracy of low-order dynamic models without increasing their complexity.

This work continues a previous study examining modifications to the basic "bicycle model" permitting prediction of a vehicle's yaw, sideslip, and roll behavior during transient maneuvers. This earlier work [5] found that, when fitting parameters for the well-known bicycle model, different combinations of driving maneuvers and algorithms can generate inconsistent estimates of cornering stiffness.

Until the present study, the mechanisms causing such inconsistency were not identified. The remainder of the paper is organized as follows: Section 2 presents preliminaries including nomenclature and model formulation. Section 3 introduces the planar bicycle and Section 4 discusses past efforts to determine tire parameters [5], specifically how these methods lead to inconsistencies in cornering stiffness estimates. Section 5 traces the source of these inconsistencies to an influence of vehicle roll on tire force, even for very small slip angles. Section 6 discusses terrain influence and how this can be removed by data pre-processing. Section 7 extends the model further to allow prediction of roll. Section 8 summarizes the results by showing the improvement in model fits to experimental data recorded in the frequency and time domains. Conclusions then summarize the main results.

PRELIMINARIES

The following notation is used for parameters in several of the models described in this work:

TABLE 1. NOMENCLATURE USED IN DYNAMIC MODELS

U	Longitudinal velocity (body-fixed frame)
m, m_s	Vehicle mass and sprung mass respectively
I_{xx}, I_{yy}, I_{zz}	Inertia about roll (X), pitch (Y), yaw (Z) axes
I_{xz}	Inertia product
l_f, l_r	Front- and Rear-axle-to-CG distances
L	Track of vehicle ($l_f + l_r$)
K_ϕ, D_ϕ	Effective roll stiffness, damping of the suspension
h	Height from roll axis to CG
α_f, α_r	Slip angles of the front, rear tires
β	Slip angle of the vehicle body at the CG
C_f, C_r	Front, Rear cornering stiffness

For ease of comparison model to model, each of the models is presented in a compact symbolic notation of the form:

$$M \cdot \ddot{q} + D \cdot \dot{q} + K \cdot q = F \cdot u_f \quad (1)$$

and

$$q = \{ y \quad \psi \quad \phi \}^T \quad (2)$$

which denotes the lateral position, yaw angle, and roll angle respectively. The input to the model,

$$u = \{ F_f \quad F_r \}^T \quad (3)$$

denotes the front and rear lateral tire forces respectively. The general MDK form described by Eq. (1) allows for an intuitive term-by-term comparison between different models and is easily transformed to standard state-space representation using transformations in presented in the authors' previous work [5].

PLANAR VEHICLE MODEL

The majority of roll models presented in the current literature, and all of the models presented in this paper, are modifications of the well-known "bicycle model." The only driver input considered in this constant-velocity model are changes in the front steering input, δ_f. While the bicycle model is a planar representation of a vehicle that ignores roll dynamics, the parameters used in the bicycle model are also commonly used in roll dynamic models [6]. This work uses SAE coordinates [11], shown in Fig. 1.

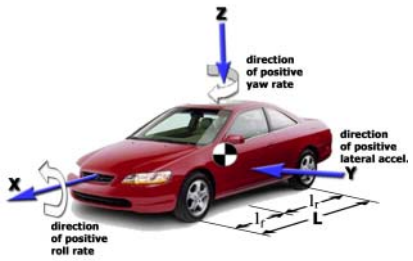

FIGURE 1: SAE COORDINATE SYSTEM

Besides restricting the vehicle to planar motion, the derivation of the bicycle model also assumes that tire forces generated on the right side of the vehicle are equal to those generated on the left side of the vehicle. This allows the vehicle to be represented as a 2-wheeled vehicle shown below.

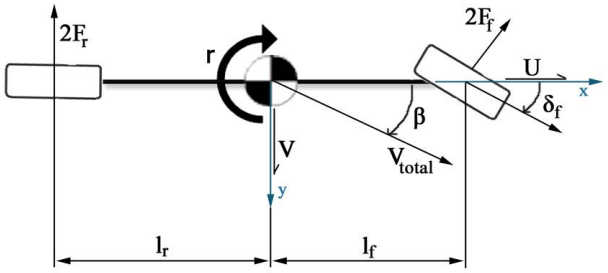

FIGURE 2: BICYCLE MODEL DIAGRAM

Summing forces in the y-direction and summing moments around the z-axis results in the equations of motion in the form of Eq. (1) with the system matrices:

$$M = \begin{bmatrix} m & 0 \\ 0 & I_{zz} \end{bmatrix}, D = \begin{bmatrix} 0 & mU \\ 0 & 0 \end{bmatrix}, K = \begin{bmatrix} 0 & 0 \\ 0 & 0 \end{bmatrix}, F = \begin{bmatrix} 1 & 1 \\ l_f & -l_r \end{bmatrix} \quad (4)$$

Detailed derivations of the bicycle model are presented in almost every vehicle dynamics text, including [7-10], and the reader is referred to these for additional detail.

Obtaining Vehicle Inertial Parameters

To analyze the ability of the models presented in this paper to describe vehicle chassis behavior, experiments were performed on a 5-door 1992 Mercury Tracer station wagon available at Penn State's Pennsylvania Transportation Institute test track. Data was collected using Novatel's GPS/INS "SPAN" system [12], a GPS/INS system that is based off two Novatel OEM4 dual frequency GPS receivers and a Honeywell HG1700 IMU. This combination provides estimates of position, velocity and attitude at rates up to 100Hz. In differential carrier, phase-fixed, integer mode, and with continuous presence of GPS data, the system achieves a position solution with an accuracy up to 2 cm. Attitude can be estimated with a 1-sigma accuracy of 0.013 degrees for roll, 0.013 deg for pitch and 0.04 degrees for yaw. All velocity errors are 0.007 m/s (one sigma).

Many of the lumped inertial parameters appearing in the dynamic models herein are easily measured or obtained from the National Highway Traffic Safety Administration database [6]. The table below presents these parameter values for the test vehicle, their units, and their source.

TABLE 2: INERTIAL PARAMETER VALUES

Variable	Value	Units	How obtained
m	1030	kg	Measured
m_s	824	kg	Estimated
W_f	6339	N	Measured
W_r	3781	N	Measured
l_f	0.93	m	NHTSA*
l_r	1.56	m	NHTSA*
L	2.49	m	Calculated
h	0.25	m	Measured
I_{zz}	1850	kg-m^2	NHTSA*
I_{yy}	1705	kg-m^2	NHTSA
I_{xx}	375	kg-m^2	NHTSA
I_{xz}	72	kg-m^2	NHTSA

*measurements were also made and these confirmed the NHTSA value to within a few percent

An estimate of the sprung mass, m_s, was obtained by approximating it as 0.8 times the total mass. The roll axis was found by video-taping the vehicle undergoing a rocking motion from the front and rear, determining the center of rotation at the front and rear axles, then using similar triangles to determine the axis of rotation at the center-of-gravity of the vehicle. The CG height was found to be 0.25 meters above the roll axis. Note that the sprung-mass height above the roll-axis is not the height of the CG above the road surface reported by NHTSA, 0.52 meters for this vehicle.

FITTING BICYCLE MODEL TIRE PARAMETERS

Several model parameters, especially the tire cornering stiffnesses, require experimental fitting and careful consideration of the tire's impact on the model behavior. The models presented in this study lump right- and left-side lateral tire forces to a single force on the front and rear axles, F_f and F_r. This single-wheel representation of a two-wheel axle is why the bicycle model is so named. Further, it is assumed that the lateral forces acting on each tire are directly proportional to the tire slip with proportionality constants on the front and rear tires of C_f and C_r respectively:

$$F_f = C_f \alpha_f, F_r = C_r \alpha_r \tag{5}$$

The slip angles, α, are defined as the angle between the tire's orientation and the velocity vector of the center of the tire:

$$\begin{aligned} \alpha_f &= \tan^{-1}\left(\frac{V + l_f \cdot r}{U}\right) - \delta_f \approx \frac{V + l_f \cdot r}{U} - \delta_f \\ \alpha_r &= \tan^{-1}\left(\frac{V - l_r \cdot r}{U}\right) \approx \frac{V - l_r \cdot r}{U} \end{aligned} \tag{6}$$

The simplifying assumptions made for Eq. (6) are that the slip angles are small enough to allow a linear approximation and that right- and left-side differences in tire forces are negligible. With these assumptions, the tire forces can be written as:

$$F_f = C_f\left(\frac{V + l_f \cdot r}{U} - \delta_f\right) \text{ and } F_r = C_r\left(\frac{V - l_r \cdot r}{U}\right) \tag{7}$$

Longitudinal forces acting upon the tires are assumed to be zero, and longitudinal velocity, U, is assumed to be constant.

The resulting expressions, when substituted into the models presented, predict linear models. However, it is well known that the linearity assumption is violated under aggressive maneuvering [13]. Therefore, care was taken in all testing to ensure that the experiments were conducted at lower accelerations.

To further test whether or not linearity is actually preserved in the measured data, two frequency responses were conducted on the vehicle. The first used steering inputs of small amplitude: 1/4 rotation of the hand wheel. The second used large amplitudes: slightly less than 1/2 rotation of the handwheel. During the steering inputs, the two states of the bicycle model, yaw rate and lateral velocity, were recorded. The vehicle was driven at a constant speed of 25 mph. The resulting Bode plots are both shown in Figs. 1 and 2 below. Both amplitudes of frequency response agree up to frequencies of 10 rad/sec, suggesting that the input-output response is approximately linear up to this frequency for input amplitudes smaller than half a rotation of the handwheel.

To find the cornering stiffnesses, two methods were used that are both based on steady-state data. Steady-state data was chosen since it is least influenced by model-to-model differences of higher-order dynamics. The first fitting method attempts to match the DC gains of the sinusoidal frequency responses of Figs. 3 and 4. The second method is based on matching measured responses from steady-state turning around a skid-pad circle. Each is described below.

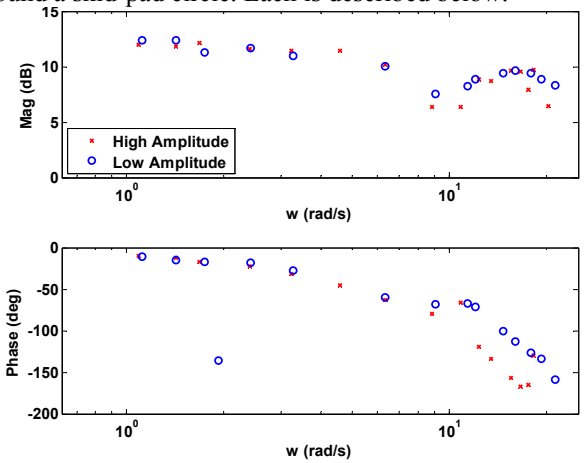

FIGURE 3: FREQUENCY RESPONSE, STEERING INPUT TO LATERAL VELOCITY

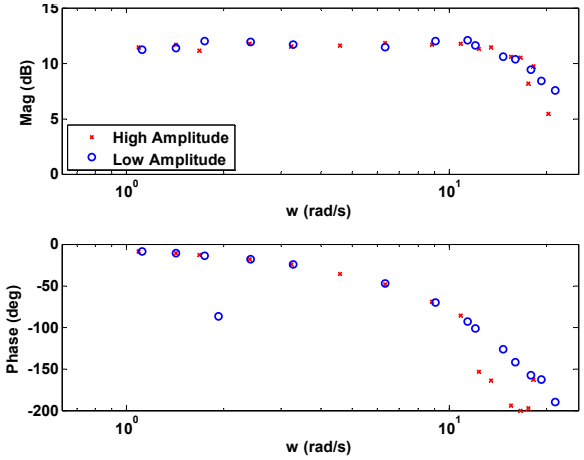

FIGURE 4: FREQUENCY RESPONSE, STEERING INPUT TO YAW RATE

The DC gains, G, of the bicycle model from steering input to state output are given by:

$$G = D - CA^{-1}B \tag{8}$$

Where A, B, C and D are the system matrices of the standard state-space form of

$$\begin{aligned} \dot{x} &= Ax + Bu \\ y &= Cx + Du \end{aligned} \tag{9}$$

For lateral velocity, V, this DC gain was parametrically solved to be:

$$G_V = \frac{U \cdot \left((C_f C_r) \cdot l_r \cdot L + C_f (l_f \cdot m \cdot U^2)\right)}{C_f C_r \cdot (l_r^2 + l_f^2 + 2 \cdot l_f \cdot l_r) + m \cdot U^2 (C_f l_f - C_r \cdot l_r)} \tag{10}$$

and for yaw rate, r:

$$G_r = \frac{U \cdot (C_f C_r) \cdot L}{C_f C_r \cdot (l_r^2 + l_f^2 + 2 \cdot l_f \cdot l_r) + m \cdot U^2 (C_f \cdot l_f - C_r \cdot l_r)} \quad (11)$$

The numerical values of G_V and G_r were read from Figs. 3 and 4 as 3.804 m/s lateral velocity per radian of steering input and 3.599 rad/sec yaw rate per radian of steering input, respectively. Hence, there are two equations and two unknowns: the front and rear cornering stiffnesses. Rearranging the above equations, one can directly solve for cornering stiffnesses after substitution of known vehicle parameters:

$$C_r = \frac{(l_f \cdot m \cdot U^2 \cdot G_r)}{(G_v - l_r \cdot G_r) \cdot L} = -88{,}385 \ \frac{\text{N}}{\text{rad}} \quad (12)$$

$$C_f = \frac{(-U^2 \cdot m \cdot G_r \cdot C_r \cdot l_r)}{(C_r \cdot U \cdot L - G_r \cdot C_r \cdot L^2 - U^2 \cdot m \cdot G_r \cdot l_f)} = -83{,}014 \frac{\text{N}}{\text{rad}} \quad (13)$$

These values, when substituted into the bicycle model, appear to match the measured sine wave time responses obtained while conducting the frequency responses. And, although the results are not shown, the model matched most time-domain maneuvers such as lane changes.

Surprisingly, the model had a very poor fit to steady-state turning responses measured on the skid pad. Fortunately, under the assumptions of the bicycle model, a constant turn steering maneuver can be used to determine cornering stiffness values. For example, steady-state turning around a constant radius circle, the side-slip, $\beta = V/U$, measured at the center-of-gravity of the vehicle is given by:

$$\beta = \frac{l_r}{R} + \frac{W_r}{C_r \cdot g} \frac{U^2}{R} \quad (14)$$

The side-slip is clearly dependent on both speed and radius of the turning circle. This therefore suggests a method to determine the rear cornering stiffness: measure side slip on the vehicle and slowly increase the vehicle speed traversing a steady circle to the point where side slip becomes zero. At $\beta = 0$, the above expression gives the rear cornering stiffness as:

$$C_r = -\frac{W_r}{l_r \cdot g} U^2 \quad (15)$$

Note that this expression is independent of the radius of the turn. Repeated measurements during steady-state circles of different radii and in opposing directions showed that the zero sideslip condition occurred repeatedly around 14.1 m/s. Using weight and length values measured for the vehicle and substituting these above, the calculated rear cornering stiffness was found to be $C_r = -49{,}300 N/rad$.

The front cornering stiffness can also be found the steady-state vehicle response. At steady-state, the steering input and front and rear cornering stiffness are related by:

$$\delta = \frac{L}{R} + \underbrace{\left(\frac{W_r}{C_r} - \frac{W_f}{C_f} \right)}_{Kus} \frac{U^2}{g \cdot R} \quad (16)$$

where $K_{us} = \left(\frac{W_r}{C_r} - \frac{W_f}{C_f} \right)$ is the understeer gradient (assuming negative cornering stiffnesses). So:

$$C_f = \frac{-W_f}{\left(\delta_f - \frac{L}{R} \right) \frac{g \cdot R}{U^2} - \frac{W_r}{C_r}} \quad (17)$$

The average steering input, δ_f, during the point at which sideslip passed through zero was approximately 0.0830 rad of front wheel angle. This gives an approximate value of $C_f = -57{,}700 \ N/rad$. This is clearly in disagreement with the results of Equation (12) and (13).

To investigate yet another means to determine the front cornering stiffness, the understeer gradient can also be used. If the rear cornering stiffness is known, the understeer is related to the front cornering stiffness by manipulation of Eq. (16):

$$C_f = \frac{W_f \cdot C_r}{W_r - C_r \cdot K_{us}} \quad (18)$$

Measurements of the understeer gradient can be obtained by plotting steering input versus lateral acceleration as shown in Fig. 5 below. Using these results, an understeer gradient was found to be $K_{us} = 0.016$. This gives a front cornering stiffness value of $C_f = -68{,}400 \ N/rad$ which is roughly 15% different from the previous value. Again, this disagrees with previous values.

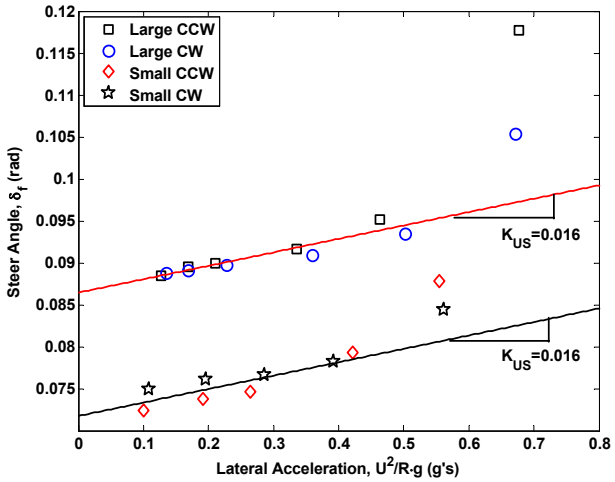

FIGURE 5: STEADY STATE STEERING MEASUREMENTS VS LATERAL ACCELERATION FOR TWO DIFFERENT RADII TURNING CIRCLES

To understand the issue further, the bicycle model responses were compared to experimental data for the cornering stiffness values in each case. When comparing the cornering stiffness values obtained from the steady-state circle methods to the steady-state circle time responses, the agreement was good. However, the same cornering stiffness values poorly matched the frequency response data. These results can be summarized as the first lesson of this work:

Lesson 1: The cornering stiffness parameter defining tire behavior is difficult to measure and may be fitted to different values depending on the maneuver used and/or the fitting technique employed.

TIRE MODEL MODIFICATIONS

To address the source of the parameter and fitting discrepancies, a further investigation into cornering stiffness values was initiated. Using data from steady state circle tests, the slip angle of the front and rear tire was calculated as was the force at each tire required to keep the vehicle moving in a steady state circle. The slip angles of each tire were plotted against the force for each axle. An example results for the rear axle is shown in Fig. 6.

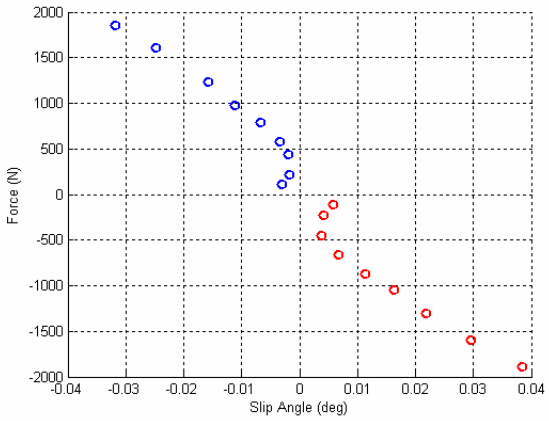

FIGURE 6. REAR TIRE SLIP ANGLE VS. REAR AXLE LATERAL FORCE

The data shows a linear relationship throughout most of the range tested which is the basis of a linear tire model, but with two obvious deviations from linearity. First, away from the origin, the line fits for force are offset producing non-zero y-axis intercepts. Second, at very low slip angles, a nonlinear relationship between slip and tire force. Both observations suggest that other factors are influencing the force predictions.

To investigate the source of this discrepancy, the tire force versus roll angle was compared as shown in Fig. 7 with tire force calculated from force and moment balance during the steady-state turn.

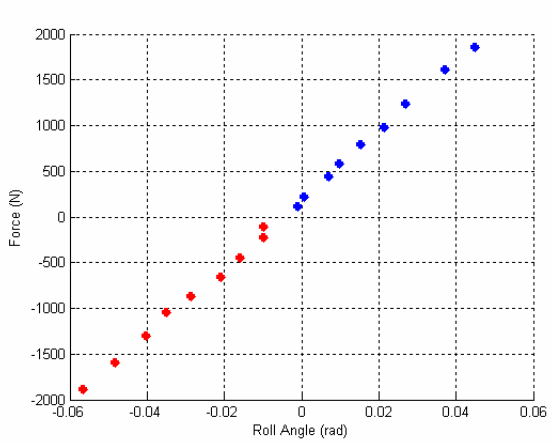

FIGURE 7. VEHICLE ROLL ANGLE VS REAR TIRE LATERAL FORCE

An interesting result was that a linear plot is produced for all values tested With these observations, it was inferred that another mechanism to produce tire force was occurring during steady turning that is strongly dependent on roll angle. Therefore, the model for tire force generation was revisited.

Lesson 2: Vehicle roll behavior can have a significant effect on tire force, especially at low lateral slip levels.

Camber Influence in Tire Forces

The previous analysis suggests that there is a significant tire force generation mechanism that is dependent on whether or not the vehicle has a roll angle. This inference is supported by Fig, 7 and the work of others. For example, in [14], Kim et al introduced a incremental change in force on the tire model in the form of $\frac{\partial \alpha_f}{\partial \phi}\phi$. This effect is commonly known as "roll steer" and is usually assumed to be a constant value when the amount of tire slip is small.

If the previous analytical methodology is applied to find the roll-steer parameters for this study, one discovers that two equations must be used to solve for four parameters – two cornering stiffnesses and two camber coefficients – to match the measured steady-state data. To make the problem solvable, one can note that the roll angles measured on a vehicle for very low frequency sine wave steering inputs are quite small. Therefore it can be assumed that the cornering stiffnesses obtained by matching the frequency responses are not greatly influenced by tire camber at low frequencies. Therefore, one only needs to consider the turning circle data to measure the influence of tire camber.

To experimentally obtain parameters representative of tire camber, the following procedure is utilized. First, the tire forces are assumed to depend on roll by the following relationship:

$$F_f = C_f \alpha_f + C_{\phi f}\phi_{wf}$$
$$F_r = C_r \alpha_r + C_{\phi r}\phi_{wr} \qquad (19)$$

where ϕ_{wf} and ϕ_{wr} are the camber angles of the front and rear tires, and $C_{\phi f}$ and $C_{\phi r}$ are the proportionality constants

representing the change in tire force as a function of roll angle. Now define the change in wheel camber angle as a function of the entire vehicle's roll angle via a proportionality constant, *S*:

$$\begin{aligned} \phi_{wf} &= S_f \cdot \phi_v \\ \phi_{wr} &= S_r \cdot \phi_v \end{aligned} \tag{20}$$

This constant encompasses linear effects due to suspension geometry, etc. for small rotations of the chassis. The steady-state roll angle of the vehicle for a constant velocity, constant radius turn, ϕ_v, is solved by moment balance:

$$\phi_v = \frac{h}{K_\phi} \cdot \frac{m_s U^2}{R} \tag{21}$$

A steady-state force balance for a vehicle traversing a steady-state turn gives the following slip angles:

$$\begin{aligned} \alpha_f &= \frac{1}{C_{\alpha f}} \left[\frac{l_r}{L} \frac{mU^2}{R} - \frac{C_{\phi f} m_s h}{K_\phi} S_f \frac{U^2}{R} \right] \\ \alpha_r &= \frac{1}{C_{\alpha r}} \left[\frac{l_f}{L} \frac{mU^2}{R} - \frac{C_{\phi r} m_s h}{K_\phi} S_r \frac{U^2}{R} \right] \end{aligned} \tag{22}$$

which can be more compactly represented as:

$$\begin{aligned} \alpha_f &= \frac{1}{S_f} \left[\frac{l_r}{L} \cdot \frac{mU^2}{R} - C_f^* \frac{U^2}{R} \right] \\ \alpha_r &= \frac{1}{S_r} \left[\frac{l_f}{L} \cdot \frac{mU^2}{R} - C_r^* \frac{U^2}{R} \right] \end{aligned} \tag{23}$$

with

$$C_f^* = \frac{C_{\phi f} m_s h}{K_\phi} S_f \text{ and } C_r^* = \frac{C_{\phi r} m_s h}{K_\phi} S_r \cdot \tag{24}$$

The steady-state steering input necessary to traverse a constant radius turn at constant speed is therefore given by:

$$\delta_f = \frac{L}{R} - \frac{1}{C_f} \left[\frac{l_r}{L} \cdot \frac{mU^2}{R} - C_f^* \frac{U^2}{R} \right] + \frac{1}{C_r} \left[\frac{l_f}{L} \cdot \frac{mU^2}{R} - C_r^* \frac{U^2}{R} \right] \tag{25}$$

which allows one to solve for the steady-state steering gains for a constant velocity, constant radius turn.

$$\left. \frac{r}{\delta_f} \right|_{circle} = \frac{\frac{U}{R}}{\frac{L}{R} - \frac{1}{C_f} \left[\frac{l_r}{L} \cdot \frac{mU^2}{R} - C_f^* \frac{U^2}{R} \right] + \frac{1}{C_r} \left[\frac{l_f}{L} \cdot \frac{mU^2}{R} - C_r^* \frac{U^2}{R} \right]} \tag{26}$$

and

$$\left. \frac{V}{\delta_f} \right|_{circle} = \frac{U \cdot \left(\frac{l_r}{R} + \alpha_r \right)}{\frac{L}{R} - \frac{1}{C_f} \left[\frac{l_r}{L} \cdot \frac{mU^2}{R} - C_f^* \frac{U^2}{R} \right] + \frac{1}{C_r} \left[\frac{l_f}{L} \cdot \frac{mU^2}{R} - C_r^* \frac{U^2}{R} \right]} \tag{27}$$

The steady-state values of these two transfer functions are easily obtained using the turning data. This allows the values of C_f^* and C_r^* to be directly calculated since all other parameters are known. For the vehicle tested in this study, these values were found to be $C_f^* = -119.50 kg$ and $C_r^* = -169.43 kg$.

Dynamic Tire Model

In previous work, examination of the phase lag observed in the frequency response data showed that a model of tire lag was necessary to obtain a reasonable model fit [5, 15]. The tire-lag phenomenon is commonly modeled as a first-order system with zero steady-state gain [9, 16]. The following model of tire lag was used which considers tire lag as a function of tire slip on the front and rear tires:

$$\begin{aligned} \frac{dF_f}{dt} &= \frac{U}{\sigma} \left(C_f \left(\frac{V + l_f \cdot r}{U} - \delta_f \right) - F_f \right) \\ \frac{dF_r}{dt} &= \frac{U}{\sigma} \left(C_r \left(\frac{V - l_r \cdot r}{U} \right) - F_r \right) \end{aligned} \tag{28}$$

The best fits were obtained with a tire lag value of sigma = 0.8 for front and 0.6 for rear, but differences between these and an average value of 0.7 were minor and so the average value is used hereafter.

TERRAIN INFLUENCES

Multiple trials of a lane change maneuvers revealed repetition in the discrepancies between the measured and predicted response from all roll models. When looking at the error plots for the same lane change at various speeds, it became clear that the variations in measured data are due to changing terrain over which the lane change was performed. This was an unexpected result, especially since these maneuvers were performed on pavement that appeared level.

To verify this hypothesized terrain-influence, cones were placed on the track to ensure repeatability of the maneuver, and the lane change was driven at 5 mph and then again at 25 mph. Data was collected during both runs and the roll data from the slow maneuver was converted to a roll vs. position table. Roll data from the low speed was assumed to be due to terrain since roll dynamics were not excited in such a slow maneuver. The measured roll angle was then corrected for terrain influence by subtracting the low speed roll value corresponding to the same position as the high speed maneuver.

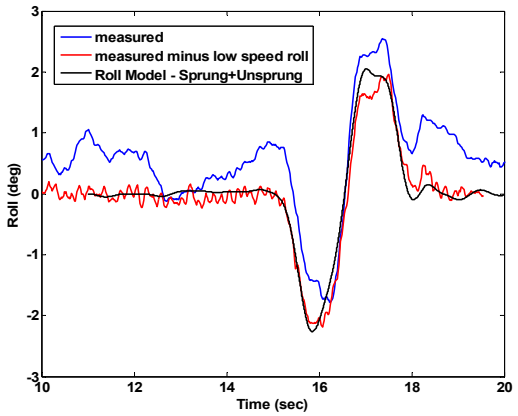

FIGURE 8: LANE CHANGE ROLL RESPONSE WITH AND WITHOUT TERRAIN COMPENSATION

A comparison is shown in Fig. 8 between raw and terrain compensated vehicle responses. The profound influence of the terrain on model fit is clearly evident.

Lesson 3: Even for seemingly "level" road conditions, terrain influence can produce easily measured errors between measured and model-predicted vehicle behavior. Subtraction of terrain influence can significantly improve model fit.

ROLL DYNAMICS MODELS

A search of recent literature found over two dozen unique vehicle models inclusive of roll dynamics. Considerations used to eliminate certain models from further study are detailed in previous work, but the main criteria were based on model complexity, whether or not the model had been validated experimentally by the authors of the model, and how easily model parameters can be measured or inferred [5, 15].

The two roll models used in this study are commonly used in the literature and the model formulations were confirmed using both Newtonian mechanics and a Lagrangian approach. The Newtonian method utilized the free-body diagram shown in Fig. 9.

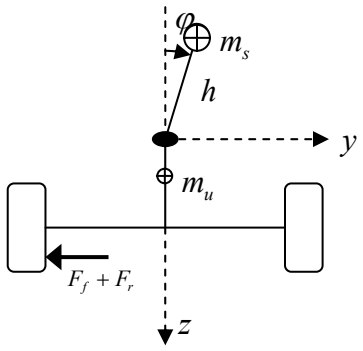

FIGURE 9. ROLL MODEL DIAGRAM

The results are similar to other published models, and have previously been compared to more complex models[5, 14, 17, 18]. The differences between the two models arise from the assumptions made about vehicle behavior. The second model assumes that the weight of the sprung mass is distributed symmetrically about the x-z plane, while the first does not. Following the MDK form of Eq. (1), the MDK matrices for both models are given by the following:

$$M_1 = \begin{bmatrix} m & 0 & m_s h \\ 0 & I_{zz} & -I_{xz} \\ m_s h & -I_{xz} & I_{xx} + m_s h^2 \end{bmatrix}, \; D_1 = \begin{bmatrix} 0 & mU & 0 \\ 0 & 0 & 0 \\ 0 & m_s h U & D_\phi \end{bmatrix} \quad (29)$$

$$K = \begin{bmatrix} 0 & 0 & 0 \\ 0 & 0 & 0 \\ 0 & 0 & K_\phi - m_s h U \end{bmatrix}, \; F = \begin{bmatrix} 1 & 1 \\ l_f & l_r \\ 0 & 0 \end{bmatrix}$$

And for the second model, which includes the above mentioned assumption, the matrices are identical except for a slightly different M matrix.

$$M_2 = \begin{bmatrix} m & 0 & m_s h \\ 0 & I_{zz} & 0 \\ m_s h & 0 & I_{zz} + m_s h^2 \end{bmatrix} \quad (30)$$

VALIDATION OF DYNAMIC MODELS

Frequency Response Tests

Only two new parameters were introduced in the modifications of the original "bicycle model" to account for roll dynamics: K_ϕ and D_ϕ. These parameters were varied manually until the models best matched the frequency response data. The resulting frequency-domain fits are seen in Figs. 10-12, where both experimental data and model are shown. The data was collected at 25 mph.

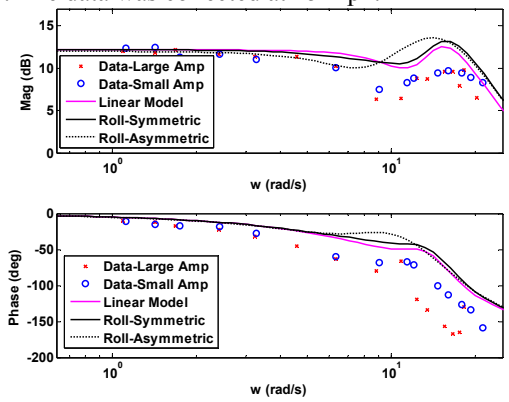

FIGURE 10: FREQUENCY RESPONSE, STEERING INPUT TO LATERAL VELOCITY

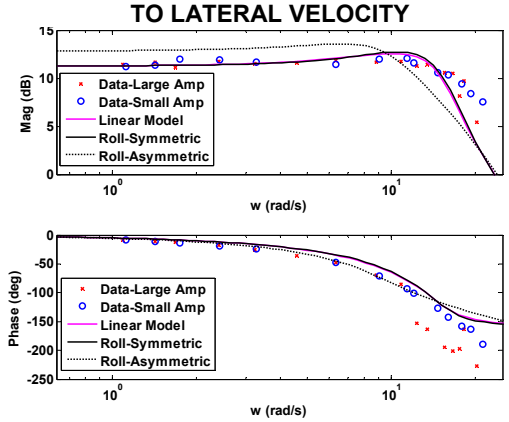

FIGURE 11: FREQUENCY RESPONSE, STEERING INPUT TO YAW RATE

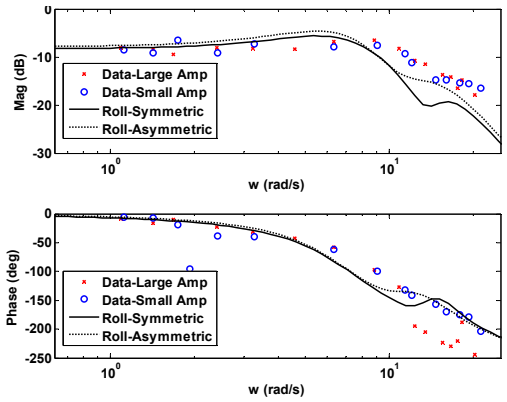

FIGURE 12: FREQUENCY RESPONSE, STEERING INPUT TO ROLL ANGLE

The most notable comment about the above fits is that they are far better than previous work [5]. The only difference between this model and previous work is the inclusion of roll influence, since subtraction of terrain effect is not possible. Particularly notable are that, unlike previous results, the shape of the model-predicted frequency responses all are in agreement with measured data. Since the curve of a frequency response is most strongly related to dynamic effects, this suggests that the primary vehicle dynamics are captured by the models. There appear slight offsets between model and experiment, particularly at high frequencies. These are likely due to slight parameter error and additional investigation of this is ongoing.

Time Response Tests

In order to obtain further understanding of the model fit obtained by the frequency response tests, time response data were also taken. Shown in Figs. 13-15 are state responses during a representative lane-change at 25 mph. These time responses all show close agreement between the models and measured data, with the largest discrepancies occurring near the peaks of the respective responses. As noted earlier, the differences between the different models appear to be quite small, much smaller than the influence of terrain of the influence of parameter fitting errors. Furthermore, the observation of a poor fit near the peaks of the frequency responses provides further indication that nonlinear effects might be influencing the data in these regions.

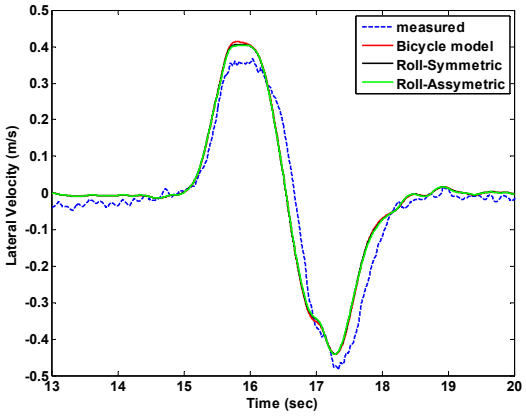

FIGURE 13: LANE CHANGE LATERAL VELOCITY RESPONSE

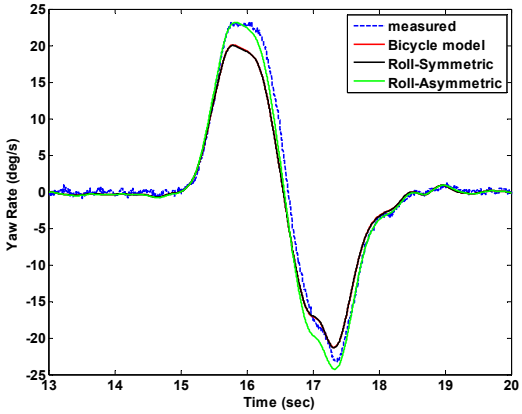

FIGURE 14: LANE CHANGE YAW RATE RESPONSE

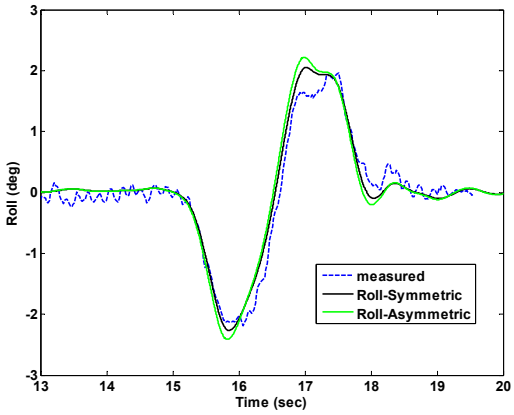

FIGURE 15: LANE CHANGE ROLL RESPONSE

CONCLUSIONS

An overview of ongoing work to model and validate vehicle roll dynamics was presented in this work particularly focusing on explaining discrepancies discovered in previous work. The results of this study can be summarized in three "lessons learned":

- Lesson 1: The cornering stiffness parameter defining tire behavior is difficult to measure and may be fitted to different values depending on the maneuver used and/or the fitting technique employed.
- Lesson 2: Vehicle roll behavior can have a significant effect on tire force, especially at low lateral slip levels.
- Lesson 3: Even for seemingly "level" road conditions, terrain influence can produce easily measured errors between measured and model-predicted vehicle behavior. Subtraction of terrain influence can significantly improve model fit.

After correcting for roll-induced tire forces and terrain effects, the resulting fits in the time and frequency domain show outstanding agreement between model and experiment.

ACKNOWLEDGEMENTS

Author Bridget Hamblin was supported by a NSF Graduate Teaching Fellowship in K-12 Education (DGE-0338240) while completing the work presented in this paper.

REFERENCES

1. *Web-based Injury Statistics Query and Reporting System (WISQARS): Years of Potential Life Lost (YPLL) Reports, 1999-2002*. 2002, The Center for Disease Control: Atlanta.
2. *Traffic Safety Facts 2005: A Compilation of Motor Vehicles Crash Data from the Fatality Analysis Reporting System and the General Estimates System*. 2006, U.S. Department of Transportation: Washington, D.C.
3. *An Experimental Examination of Selected Maneuvers That May Induce On-Road, Untripped, Light Vehicle Rollover - Phase II of NHTSA's 1997-1998 Vehicle Rollover Research Program: NHTSA Report HS 808 977*. 1999, U.S. Department of Transportation.
4. *A Comprehensive Experimental Examination of Selected Maneuvers That May Inducse On-Road, Untripped, Light Vehicle Rollover - Phse IV of NHTSA's Light Vehicle Rollover Research Program: NHTSA Report HS 809 513*. 2002, U.S. Department of Transportation.
5. Hamblin, B.C., Martini, Ryan D., Cameron, John T., Brennan, Sean N. *Low-Order Modeling of Vehicle Roll Dynamics*. in *American Control Conference*. 2006.
6. Heydinger, G.J., Bixel, Ronald A., Garrott, W. Riley, Pyne, Michael, Howe, J. Gavin, Guenther, Dennis A. *Measured Vehicle Interial Parameters - NHTSA's Data Through November 1998 : SAE 1999-01-1336*. 1999.
7. Bundorf, R.T., *A Primer on Vehicle Directional Control*. 1968, Warren: General Motors Technical Center: Michigan Engineering Publication.
8. Gillespie, T.D., *Fundamentals of Vehicle Dynamics*. 1992, Warrendale: SAE Press.
9. Karnopp, D., *Vehicle Stability*. 2004, New York: Marcel Dekker, Inc.
10. Pacejka, H.B., *Tire and Vehicle Dynamics*. 2006, Warrendale: SAE Press.
11. *SAE J670e 1976 Vehicle Dynamics Technology*. 1976, Warrendale, PA: Society of Automotive Engineers, Inc.
12. Cameron, J.T., Brennan, Sean N., *Vehicle Dynamic Modeling for the Prediction and Prevention of Vehicle Rollover*, in *Mechanical Engineering*. 2005, Pennsylvania State University: University Park.
13. LeBlanc, D.J., Johnson, G.E., Venhovens, P.J., Gerber, G., DeSonia, R., Ervin, R., Lin C-F., Ulsoy, A.G., Pilutti, T.E., *CAPC: A Road-Departure Prevention System.* IEEE Control Systems Magazine, 1996: p. 61-71.
14. Kim, H.-J., *Investigaton of Robust Roll Motion Control Considering Varying Speed and Acuator Dynamics.* Mechatronics, 2004. **14**(1): p. 35-54.
15. Cameron, J.T., Brennan, Sean N., *A Comparitive, Experimental Study of Model Suitability to Describe Vehicle Rollover Dynamics for Control Design.* ASME Dynamic Systems and Control Division, 2005. **74**(1): p. 405-414.
16. Heydinger, G.J., Garrott, W. Riley, Chrstos, Jeffrey P., Guenther, Dennis A., *Dynamic Effects of Tire Lag on Simulation Yaw Rate Predictions.* Jounal of Dynamic Systems, Measurement and Control, 1994. **116**(2): p. 249-256.
17. Carlson, C.R., Gerdes, J. Christian, *Optimal Rollover Prevention with Steer by Wire and Differential Braking.* ASME Dynamic Systems and Control Division, 2003. **72**(1): p. 345-354.
18. Mammar, S. *Speed Scheduled Vehicle Lateral Control*. in *IEEE Conference on Intelligent Transportation Systems*. 1999.